International Journal of Nanomedicine Dovepress

Open Access Full Text Article ORIGINAL RESEARCH

Icariin-Enhanced Osteoclast-Derived Exosomes Promote Repair of Infected Bone Defects by Regulating Osteoclast and Osteoblast Communication

Yang Zhang[1], Minjie Zhang[2], Mengying Li[2], Maomao Miao[2], Dan Shou[2], Peijian Tong[1]

[1]Institute of Orthopaedics and Traumatology, The First Affiliated Hospital of Zhejiang Chinese Medical University (Zhejiang Provincial Hospital of Chinese Medicine), Hangzhou, 310053, People's Republic of China; [2]School of Pharmaceutical Sciences, Zhejiang Chinese Medical University, Hangzhou, 310053, People's Republic of China

Correspondence: Dan Shou; Peijian Tong, Email shoudanok@163.com; peijiantong@zcmu.edu.cn

International Journal of Nanomedicine downloaded from https://www.dovepress.com/
For personal use only.

Background: Infected bone defects pose a challenging clinical issue due to an imbalance of osteoclasts (OC) and osteoblasts (OB). Exosomes are crucial for intercellular signaling of OC and OB in bone repair. Icariin, has been shown to regulate the balance between OC and OB. However, the specific mechanisms by which icariin influences exosomes derived from osteoclasts, and subsequently impacts osteoblast activity, remain unclear. This study aims to investigate the effects of icariin-treated osteoclast-derived exosomes (ICA-OC-Exo) on osteoblast function and bone repair in cases of infected bone defects.

Methods: We investigated the exosome profile and localization of multivesicular bodies (MVB) and quantification of intraluminal vesicles (ILVs) in osteoclasts by using transmission electron microscopy. Additionally, the expressions of Rab27A and MITF, which are associated with exosome release, were determined through immunofluorescence staining and Western blot. The profiling of exosomal miRNA expression was conducted via miRNA-sequencing. The effects of ICA-OC-Exo on osteoblast differentiation were determined using RT-qPCR, Western blot, alkaline phosphatase staining. Additionally, ICA-OC-Exo was administered into the localized bone defect of the infected bone rat models, and bone formation was assessed using Micro-CT.

Results: Icariin increased the presence of MVBs in the cytoplasm through modulation of the MITF/Rab27A signaling pathway, resulting in higher number of ICA-OC-Exo compared to OC-Exo. Additionally, miR-331-3p expression in ICA-OC-Exo was found to be elevated compared to OC-Exo. ICA-OC-Exo was observed to stimulate osteoblast function by targeting FGF23, reducing DKK1, and subsequently upregulating ALP. In the in vivo study, ICA-OC-Exo exhibited the capacity to enhance bone healing at the site of a local bone defect following anti-infection treatment.

Conclusion: Icariin enhanced the quantification of OC-Exo and the expression of miRNA-331-3p in OC-Exo, leading to the regulation of osteoblast function via activation of the miRNA-331-3p/FGF23/DKK1 pathway. ICA-OC-Exo demonstrated potential clinical applicability in bone repair of infected bone defects.

Keywords: infected bone defects, icariin, osteoclast, exosomes, osteoblast

Introduction

Infected bone defects represent a prevalent complication of traumatic orthopedic surgery, often stemming from acute blood-borne or chronic osteomyelitis, traumatic or postoperative infections, or bone tumors.[1] With the advancement of the economy and transportation infrastructure, high-energy injuries related to road traffic have become increasingly prevalent. Annually, approximately 50 million individuals suffer injuries as a result of traffic accidents or earthquakes, contributing to a significant number of patients experiencing infected bone defects.[2] These defects pose a significant challenge within the medical field due to the prolonged treatment duration, elevated costs, and high recurrence rates.[3,4] Current therapeutic approaches for managing infected bone defects predominantly encompass surgical debridement

Received: 20 June 2024
Accepted: 8 November 2024
Published: 21 November 2024

© 2024 Zhang et al. This work is published and licensed by Dove Medical Press Limited. The full terms of this license are available at https://www.dovepress.com/terms.php and incorporate the Creative Commons Attribution – Non Commercial (unported, v3.0) License (http://creativecommons.org/licenses/by-nc/3.0/). By accessing the work you hereby accept the Terms. Non-commercial uses of the work are permitted without any further permission from Dove Medical Press Limited, provided the work is properly attributed. For permission for commercial use of this work, please see paragraphs 4.2 and 5 of our Terms (https://www.dovepress.com/terms.php).

Graphical Abstract

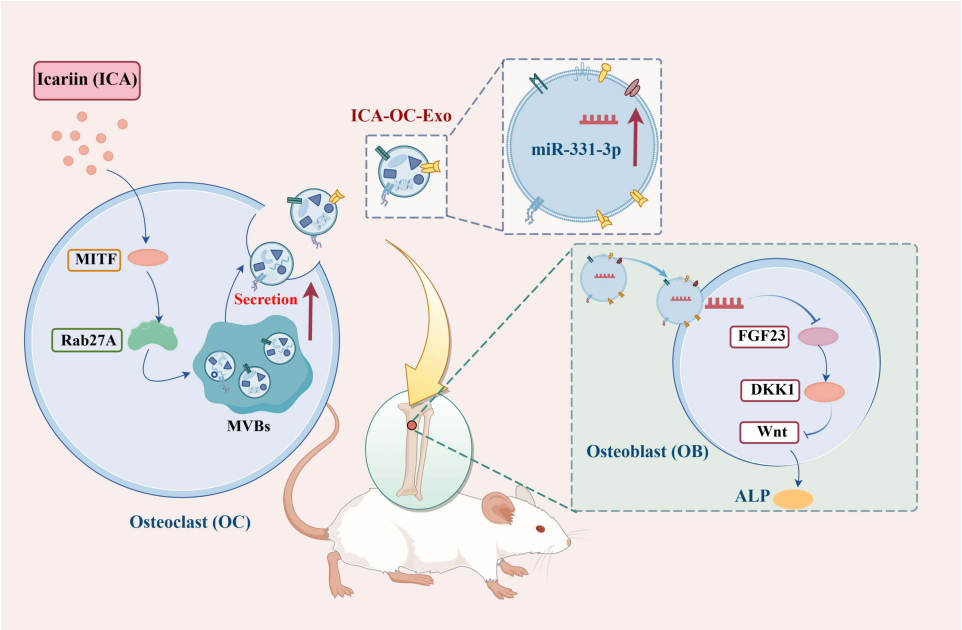

combined with the implantation of antibiotic delivery systems, generally yielding a high success rate.[5] Nonetheless, approximately 20% of cases experience treatment failure despite these interventions.[6] Treating infected bone defects is complicated by antimicrobial resistance, antibiotic tolerance from metabolic changes or biofilms, poor antibiotic penetration in compromised bone, and colonization in protected bone reservoirs.[7,8] The failure to treat infected bone defects ultimately causing serious disability and significantly impacting their quality of life.[6,9] Therefore, the management of infected bone defects necessitates a focus on bone repair and reconstruction.

A comprehensive investigation into infected bone defects was undertaken through a combination of clinical and basic research studies.[10,11] Osteoblasts (OBs) and osteoclasts (OCs) are responsible for bone formation and resorption, respectively. These cells interact through a coupling mechanism to achieve a dynamic equilibrium, thereby maintaining normal bone mass.[12] Our team's findings revealed a notable increase in osteoclast activity and a decrease in osteoblast activity within bone tissue samples obtained from individuals with infected bone defects.[13,14] Exosomes, a type of extracellular vesicle ranging in size from 30 to 150 nm, were identified as carriers of various bioactive substances such as proteins, mRNA, and microRNA (miRNA). These exosomes are released by donor cells and have the ability to impact the biological functions of neighboring receptor cells upon entry.

Exosomes contain significant amounts of miRNAs, which are transported to receptor cells to control the translation of target mRNA and contribute to the pathophysiological mechanisms of these cells.[15] Rab proteins control exosome secretion by recruiting specific receptor proteins on the plasma membrane. Different Rab proteins regulate different stages of secretion, with Rab27A promoting fusion of MVB with the plasma membrane.[16] Microphthalmia-associated transcription factor (MITF) regulates the gene expression of Rab27A, which controls melanosome distribution and exocytosis in melanoma cells.[17] This suggests that MITF/Rab27A is an important pathway regulating exosomes secretion into the extracellular cell of osteoclasts. Previous studies showed that osteoclasts can transport miRNAs to osteoblasts via exosomes, which enter through mechanisms like membrane fusion, endocytosis, and receptor interactions. These exosomes release miRNAs, affecting gene expression and osteoblast function.[18–20]

Recent research has shown that the sorting and packaging of miRNAs into exosomes is selective.[21] Factors like hypoxia and inflammation, as well as small molecules or traditional Chinese medicine extracts, can change the miRNA

components in bone cell exosomes, impacting bone repair and reconstruction.[22] Icariin, the principal bioactive constituent of *Herba Epimedii*, has been shown to suppress osteoclastogenesis in ovariectomized mice. Pharmacological studies have further demonstrated that icariin not only enhances the osteogenic differentiation of bone marrow mesenchymal stem cells and increases osteoblast activity, but also inhibits osteoclast differentiation and the bone resorption activity of mature osteoclasts.[23,24] In other studies, it has been demonstrated that icariin is transported by fetal bovine serum-exosomes for the treatment of bone loss conditions.[25,26] Furthermore, mesenchymal stem cells loaded with icariin-exosomes exhibited enhanced cartilage preservation.[27] Building upon previous studies, icariin demonstrates potential in augmenting bone repair processes by modulating the interactions between osteoclasts and osteoblasts via exosome-dependent pathways. However, the specific mechanism of icariin influence osteoclast-derived exosomes to enhance osteoblast activity is unclear and needs further investigation.

Consequently, we hypothesize that icariin may modulate the release of characteristic exosomes and microRNAs from osteoclasts, thereby enhancing osteoblast activity through intercellular communication between osteoclasts and osteoblasts, ultimately facilitating the repair of infected bone defects. To validate this hypothesis, the present study examines the therapeutic mechanisms of exosomes derived from icariin-treated osteoclasts (ICA-OC-Exo). MiRNA sequencing was utilized to identify highly expressed miRNAs in ICA-OC-Exo. Subsequently, ICA-OC-Exo was administered into bone defects in rat models with bone infections following anti-infection treatment, and the efficacy of bone repair was assessed. Our findings demonstrate the selective sorting of specific miRNAs in exosomes derived from icariin-regulated osteoclasts, and propose a novel approach for utilizing ICA-OC-Exo in the treatment of infected bone defects. We anticipate that ICA-OC-Exo could serve as a valuable tool for facilitating bone repair following antibiotic treatment of infected bone defects, addressing the current lack of effective methods for promoting bone regeneration.

Materials and Methods

Cell Culture and Treatment

Bone marrow macrophages (BMMs) were obtained from the long bones of 6-week-old C57BL/6 mice. The animal study was reviewed and approved by Animal Ethics Committee of Zhejiang Academy of Traditional Chinese Medicine, and conformed to Laboratory Animal-Guideline for ethical review of animal welfare (GBT 35892–2018). BMMs were cultured in α-MEM supplemented with 10% heat-inactivated fetal bovine serum, and treated with M-CSF. Osteoclasts were generated from BMMs by plating 5×10^4 cells per well in 24-well or 6-well plates and culturing them in the presence of 40 ng/mL M-CSF and 40 ng/mL purified glutathione S-transferase-RANKL as specified in individual experiments.[28] Osteoclasts were then stained for TRAP expression using a TRAP stain kit (KGA221, KEYGEN, China). The osteoclasts were treated with icariin of concentrations at 10 μg/mL 20 μg/mL, and 40 μg/mL.

The MC3T3-E1 cell line, procured from the National Collection of Authenticated Cell Cultures (Shanghai, China), was employed as a representative model of osteoblasts based on a previous study.[29] Osteoblasts utilized in the experiment were cultured in α-MEM medium (Genomcell bio; China) supplemented with 10% fetal bovine serum. The osteoblasts were cultured in a humidified incubator at 37°C with a gas mixture of 95% air and 5% CO_2, with the culture medium replenished every 2–3 days, and the passage four osteoblasts were used for all the cellular function tests. Upon reaching 80% confluency, the ICA-OC-Exo and OC-Exo were introduced to the osteoblasts, followed by cell harvesting, counting, and preparation for subsequent analysis.

Electron Microscopy Investigation of MVBs in Osteoclasts

Osteoclasts were cultured on dishes, washed in PBS, and fixed in 2.5% glutaraldehyde in 0.1M phosphate buffer for 1 hour at room temperature. The cells were then gently scraped, pelleted in Eppendorf tubes, washed in PBS, and incubated with 1% sectioned using a Leica ultramicrotome (Leica Microsystems). Ultrathin sections (50–70 nm) were stained with 2% uranyl acetate and a lead-staining solution before being observed using a transmission electron microscope (TEM) (H-7650, HITACHI, Japan). The quantitative analysis of MVBs and ILVs was carried out using ImageJ software. For each experiment, at least 6 MVBs were analyzed from separate cells.

Molecular Docking

AutoDock Vina (Vina, version 1.1.2) was used to analyze the binding activity between icariin and the target MITF. The structure of icariin was obtained from PubChem, and the MITF protein from UniProt (ID Q08874). Icariin was the ligand and MITF was the receptor. AutodockTools were used for hydrogenation, charge checking, atomic type designation, and building docking grids for protein structures. A conversion from the PDB format to the PDBQT format is then required. After Vina docking, binding strength and activity are determined for MITF and icariin. In the crystal structure, the ligand was pivotal in determining the central site of the docking grid box, which was defined by xyz dimensions of 40 Å × 40 Å × 40 Å. An exhaustiveness parameter of 8 was selected for ligand docking at this specified grid center. Following the identification of the docking pocket coordinates, molecular docking and conformational scoring were performed. Lower scores indicate greater stability of the compound's binding to the target, offering an initial assessment of icariin's binding affinity to MITF. Pymol and Discovery Studio software were used for 3D and 2D force analysis and visualization.

Exosomes Isolation

To diminish the impact of exosomes in fetal bovine serum (FBS), exosomes were removed from FBS through ultracentrifugation at 200,000 g at 4 °C for 16 hours. The resulting supernatants were then filtered through a 0.22 μm sterile filter and combined with serum-free media to create exosome-depleted cell culture media with a 10% FBS concentration. Cells were cultured in this exosome-depleted media until reaching 70% confluence.

Exosomes were harvested from culture supernatant by collecting cell culture media from osteoclasts and subjecting it to sequential centrifugations in an ultracentrifuge (XPN100, Beckman Coulter, USA) to remove debris and non-exosome vesicles. The media underwent centrifugation at 300 × g and 2000 × g for 10 minutes to eliminate dead cells and cell debris, followed by centrifugation at 10,000 × g for 30 minutes to eliminate large vesicles. Finally, exosomes were isolated by centrifugation at 110,000 × g for 70 minutes. The final pellets were used directly or resuspended in PBS buffer and stored at −80 °C for following experiments.

Identification and Characterization of Exosomes

Exosomes were examined via transmission electron microscopy (TEM) utilizing negative staining. A droplet of exosomes was deposited onto a copper grid for duration of 1 minute, subsequently desiccated at 30 °C, and scrutinized using a TEM instrument with an acceleration voltage of 120 kV. The concentration and size of the isolated exosomes were quantified employing Nanoparticle Tracking Analysis (NTA). A 405 nm monochromatic laser was directed at the exosome suspension diluted with phosphate-buffered saline (PBS). Particle motion was analyzed using NTA software, with each individual particle being identified and tracked. Brownian motion was monitored and quantified, and the Stokes-Einstein equation was applied to calculate the particle size based on the velocity of particle motion. This allowed for the determination of the visualized nanoparticle diameter and relative concentration. The evaluations of the samples were conducted in triplicate. Exosomes from various batches were collected, and their concentrations were quantified utilizing the Bicinchoninic Acid (BCA) assay. Subsequently, an equivalent quantity of protein that is specific to exosomes was isolated through the process of electrophoresis on a gel made of polyacrylamide and sodium dodecyl sulfate. The protein is transferred to a PVDF membrane, blocked with 5% skim milk, and incubated overnight at 4 °C with antibodies CD9, CD63, CD81, and Calnexin. The next day, a secondary antibody is applied for 2 hours at room temperature, followed by ultra-sensitive ECL exposure and imaging.

Co-Culture of OC-EXO and Osteoblasts

In order to evaluate the impact of osteoclast-released exosomes on osteoblasts, osteoblasts were cultured in 6-well plates at a density of 1.5×10^5 cells per well. Following cell attachment, the culture media was replaced with fresh media containing 20 μg/mL of osteoclast-derived exosomes, quantified using the Bicinchoninic acid (BCA) assay. Osteoblasts were seeded in a six-well plate at a density of 5×10^5 cells/mL. Upon reaching 60% confluence, the cells were cultured in Opti-MEM (Grand Island Biological Company, USA) and subsequently transfected with a negative control (N.C.) and miRNA-331-3p inhibitor. Following transfection, the culture medium was replaced with fresh medium and incubated for either 24 or 48 hours at 37° C in a 5% CO_2. Subsequently, OC-Exo and ICA-OC-Exo were introduced into the culture medium.

The exosomes were fluorescently labeled with PKH67 (UR52302, Umibio, China) as per the manufacturer's instructions, wherein the isolated exosomes from 200 mL of culture media were resuspended in 500 μL of Diluent C and 4 μL of PKH67 was diluted in another 500 μL of Diluent C. Subsequently, the two solutions were gently mixed for 5 minutes, followed by the addition of 5 mL of 1% bovine serum albumin to bind the excess dye. The resulting mixture was then subjected to ultracentrifugation at 100,000 g for 2 hours at 4 °C, washed with PBS via ultracentrifugation, and ultimately resuspended in complete medium. Exosomes without PKH67 staining were prepared as the negative control. The exosomes were stained with PKH67 for 30 minutes at 37 °C. Following a 24-hour co-culture, the incorporation of exosomes into osteoblasts was observed under a fluorescence microscope (Olympus-CX41, Olympus, Japan).

ALP Staining for Osteoblasts

The ALP staining technique was utilized to assess the differentiation potential of osteoblast cells. Osteoblasts were cultured in six-well plates and exposed to designated treatments. After a 24-hour treatment duration, cells were rinsed thrice with chilled PBS, fixed with 4% paraformaldehyde at 37°C for 10 minutes. A dye solution was then applied, and the samples were incubated in the dark for 1 hour. Finally, the staining patterns of the cells on the samples were documented using a digital camera. The staining was performed using the ALP staining kit (20220306, KGI Biotechnology, China). For the analysis of ALP activity, cell lysates were isolated using a cell lysis buffer on day 7. A substrate buffer with 5 mmol/L p-nitrophenol was added, and samples were incubated at 37°C for 15 minutes. Absorbance was measured at 520 nm, and ALP activity was normalized to protein content measured at 562 nm.

RT–qPCR

Total RNA from exosome cells was isolated using TRIzol reagent (H818KA1304, Sangon Biotech, China). The concentration of total RNA was identified with a spectrophotometer (NanoDrop 2000, Thermo Scientific, MA, United States), and RNA purity was determined by the A260/280 ratio range of 1.8–2.1. Then, cDNAs were synthesized following the reverse transcription kit instructions (Sangon Biotech, BSB09M1; BIOFLUX, B532453-0020). The fluorescence quantitative PCR system was performed as follows: Total RNA in the cells in exosomes was isolated using TRIzol reagent (H818KA1304, Sangon Biotech, China) and cDNAs were compounded according to the instructions of the reverse transcription kit (Sangon Biotech, BSB09M1; BIOFLUX, B532453-0020). The sequences of the primers used in this study are listed in Table 1. The fluorescence quantitative PCR system was performed as follows: for mRNA: Mix SYBR Premix, primers, cDNA, and ddH_2O. For miRNA: Mix miRNA qPCR master mix, primers, ROX Reference, cDNA, and ddH_2O. Analyze gene expression using the $2^{-\Delta\Delta}$ CT method on a 7500 fluorescent quantitative PCR instrument. The primers sequences of miRNA-331-3p and U6 are listed in Table 1.

Western Blot Analysis

Cells were lysed in RIPA lysis buffer (20220708, KeyGEN, China) and centrifuged to obtain the supernatant. Total protein was quantified using a BCA Protein Assay Kit (20220517, KeyGEN, China). Equal amounts of protein were separated by gel electrophoresis, transferred to PVDF membranes, and blocked with bovine serum albumin. Following incubation with primary antibodies against TRAP (Bioss, PB0880, 1:1000), MITF (Bioss, BS-1990R, 1:1000), Rab27A (Affinity, DF6702, 1:1000), ALP (Bioss, bsm-522526, 1:1000), or GAPDH (Bioss, BM3874, 1:1000) at 4 °C overnight,

Table 1 Primer Sequence for RT-qPCR

Gene	Forward (5′ -3′)	Reverse (5′ -3′)
miRNA-331-3p	5′-CGGCCCCTGGGCCTATC-3′	5′-AGTGCAGGGTCCGAGGTATT-3′
U6	5′-CTCGCTTCGGCAGCACATATACT-3′	5′-ACGCTTCACGAATTTGCGTGTC-3′
FGF23	5′-CAGGAGCCATGACTCGAAGGTTC-3′	5′-AGGTAGTGATGCTTCTGCGACAAG-3′
DKK1	5′ -GCCTCCGATCATCAGACGGT-3′	5′-GCAGGTGTGGAGCCTAGAAG-3′
ALP	5′ -CGGCGTCCATGAGCAGAACTAC-3′	5′-CAGGCACAGTGGTCAAGGTTGG-3′
β-actin	5′ -CTGAGAGGGAAATCGTGCGTGAC-3′	5′-ACCGCTCGTTGCCAATAGTGATG-3′

HRP-conjugated secondary antibodies (Abcam, 1054, 1:2000) were applied for 1 hour. Subsequently, the PVDF membranes were visualized using a ChemiDocTM MP Imaging system (BioRad Co., Ltd., CA, USA) and analyzed with Image J software.

Infected Bone Nonunion Rat Model and Treatment

Male SD rats weighing 300g ±20g were kept in standard animal housing conditions with a 12-hour light-dark cycle and access to food and water. The rat models were prepared as described previously.[30] A 1mm diameter bone defect was created at the tibial plateau and filled with bone wax, followed by injection of 0.1mL *S. aureus* suspension with a concentration of 1×10^6 CFU/mL into the bone marrow. The male SD rats (300g ±20g weight) were maintained under standard animal housing conditions (12-h light, 12-h dark cycles and free access to food and water). The rat models were prepared were according to previous methods. A bone defect of 1 mm diameters was punched at tibial plateau; the holes were filled with bone wax, then 0.1 mL *S. aureus* suspension (China General Microbiological Culture Collection Center, CGMCC) with the concentration of 1×10^6 CFU/mL was injected into the bone marrow by penetrating the bone wax layer. After a three-week period following infection, the rats were found to have developed bone infections. Subsequently, the rats underwent debridement by creating two adjacent 2-mm-diameter holes at the sites of infection, followed by the implantation of Van-CS (1mg per rat) into the holes. The rats were then divided into groups, namely the Van-CS group, the Van-CS+OC-Exo group, and the Van-CS+ICA-OC-Exo group. Rats in the Van-CS+ICA-OC-Exo group and Van-CS+OC-Exo group received local injections of ICA-OC-Exo or OC-Exo at a dosage of 0.2mg/kg twice a week, and for a duration of 6 weeks. At the 3-week and 6-week marks, the rats were euthanized, and their tibiae were harvested for evaluation of treatment effects.

Microcomputed Tomography

The tibias isolated from the rats were scanned by micro computed tomography (micro-CT) system (μCT-100 SCANCO Medical AG, Switzerland) according to previous protocols.[31] Bone formation indexes such as ratio of bone volume/tissue volume (BV/TV), and bone mineral density (BMD) were obtained and analyzed from the 3D model.

Immunofluorescence Analysis

Following deparaffinization, rat tibia slices underwent permeabilization, blocking, and overnight incubation at 4 °C with anti-OCN (1:200, Bioss, bs-0470R) and anti-FGF23 (1:100, Abcam, ab98000) antibodies. On the following day, 2-hour incubation of the corresponding secondary antibody was conducted at room temperature in the dark. Following an additional PBS wash, the slices were mounted using a DAPI-containing mounting medium. Imaging was conducted using a 3D digital slicing scanner (3DHISTECH's PANNORAMIC DESK/MIDI/250/1000) and software (CaseViewer2.4) for image acquisition. For each analysis, a minimum of three sections/wells were chosen, and five visual fields were randomly examined from each section/well. 100 cells were counted in each field, and the percentage of positive cells was subsequently calculated.

Statistical Analysis

Means and standard deviations were utilized to represent the quantitative data in this study. Statistical analysis was conducted using SPSS 20.0 and GraphPad Prism 8.0 to perform an analysis of variance (ANOVA) and a least significant difference *t*-test. Group differences were assessed through a two-way ANOVA followed by a Bonferroni post hoc test, with statistical significance set at $P < 0.05$ and $P < 0.01$. All experimental results were expressed as the mean value and standard error of more than three repetitions.

Results

Icariin Regulate Osteoclasts Activity and MVBs Formation in Osteoclasts

Osteoclasts induced by RANKL and M-CSF were exposed to icariin at concentrations of 10μg/mL, 20μg/mL, and 40 μg/mL. The control group exhibited the typical multinuclear structure of osteoclasts through TRAP staining (Figure 1A). Treatment

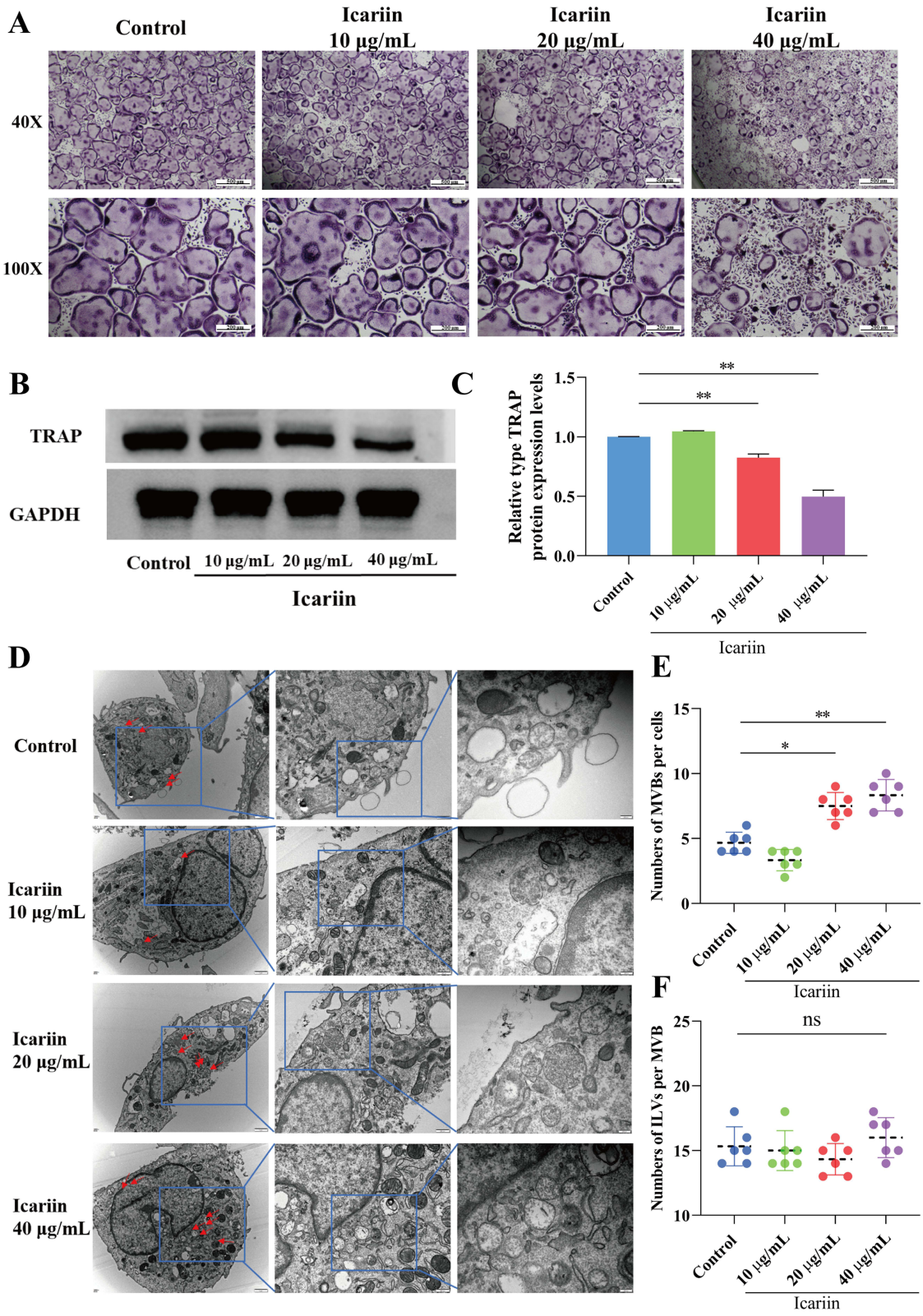

Figure 1 Icariin regulated osteoclasts activity and MVBs formation in osteoclasts. (**A**) The images of TRAP staining for osteoclasts in different concentration of icariin treatment groups (Magnification ×40 and ×100). (**B** and **C**) Western blot analysis of TRAP expressions in osteoclasts in different groups. $^{**}P < 0.01$ compared with the control group. (**D**) Transmission electron microscopy images showing representative fields with MVBs (red arrows) and in osteoclasts treated with different concentration of icariin (Magnification ×25000 and ×50000). (**E**) The quantification of MVB numbers in osteoclasts. Each dot represents the number of MVBs per section and mean is indicated in black dotted lines. $^{*}P < 0.05$, $^{**}P < 0.01$ compared with the control group. (**F**) The histogram represents the quantification of ILV numbers per MVB in osteoclasts by treating with different concentration of icariin.

with 20μg/mL and 40 μg/mL icariin resulted in inhibition of osteoclast formation compared to the control group. The expression of TRAP protein was decreased by treatment with 20μg/mL and 40 μg/mL icariin (Figure 1B and C).

Cells release various exosomes, which originate from either direct evagination of the plasma membrane or from endosomal compartments known as MVBs. Transmission electron microscopy (TEM) was utilized to examine the formation of multivesicular bodies (MVBs) in osteoclasts. In the groups treated with 20μg/mL and 40 μg/mL of icariin, a significant accumulation of MVBs was observed surrounding the plasma membrane of osteoclasts. In contrast, MVBs were found to be localized around the nucleus rather than the plasma membrane in the control groups. The quantity of MVBs per cell was found to be elevated in the 20μg/mL and 40 μg/mL icariin treatment groups (Figure 1D and E). The membrane of MVBs undergoes invagination to generate intraluminal vesicles (ILVs), which are subsequently released into the extracellular milieu upon fusion of MVBs with the plasma membrane. The ILVs in MVBs were quantified, revealing no statistically significant variance in ILV quantity per MVB in the treated osteoclasts (Figure 1F). These findings suggest that icariin suppresses osteoclast activity, enhances MVB numbers within the cytoplasm, and facilitates the fusion of MVBs with the plasma membrane.

Icariin Regulated MITF/Rab27A in Osteoclasts

The interaction between Icariin and MITF resulted in a binding energy of −6.0 kcal/mol, indicating stable binding. Analysis of a 3D diagram (Figure 2A) revealed that Icariin formed two hydrogen bonds at distances of 2.9 Å and 3.9 Å with the 330 ARG and 334 Leu residues of the MITF protein, respectively. Additionally, two hydrophobic forces at distances of 3.8 Å and 4.0 Å were observed to interact with the 337 LEU residue of MITF protein. Furthermore, two hydrophobic forces at distances of 3.9 Å and 3.5 Å were involved in binding to the 338 ILE and 361 Ile residues of the MITF protein, respectively. Two hydrophobic interactions, measuring 3.3 Å and 3.7 Å, were utilized to interact with the 364th leucine (LEU) amino acid residue of the MITF protein. Similarly, the 361st isoleucine (ILE) amino acid residues of MITF were engaged by two hydrophobic interactions measuring 3.6 Å and 3.8 Å. The 365th amino acid residue (glutamine, Gln) of MITF was bound by a 3.7 Å hydrophobic interaction and a 3.8 Å hydrogen bond. Additionally, a 3.0 Å hydrogen bond was employed to bind to the 368th glutamine (GLN) amino acid residue of MITF. The presence of these interactions facilitated the stable binding of icariin to MITF.

The small GTPase RAB27A plays a crucial role in the formation, trafficking, and membrane fusion of multivesicular bodies (MVBs). Recent research has identified RAB27A as a direct transcriptional target of MITF.[12] Immunofluorescence staining of cytoskeleton with phalloidin and nuclei with DAPI revealed that in control groups, Rab27A was distributed in the cytoskeleton and cytoplasm. It is hypothesized that MITF plays a role in the regulation of Rab27A and facilitates the extracellular secretion of multivesicular bodies (MVBs). Immunofluorescence staining results of MITF demonstrated an upregulation of MITF expression in osteoclasts treated with icariin (Figure 2B and C). Conversely, in groups treated with 20μg/mL and 40 μg/mL of icariin, Rab27A was predominantly localized in the cytoplasm. The colocalization Pearson correlation coefficient (PCC) analysis revealed that Rab27A exhibited a tendency to localize away from the cytoskeleton following treatment with 20μg/mL and 40 μg/mL icariin. Furthermore, the effect was more pronounced with the 40 μg/mL icariin treatment compared to the 20 μg/mL treatment (Figure 2D and E). The protein expression levels of MITF and Rab27A were found to be significantly upregulated by 20μg/mL and 40 μg/mL of icariin, as shown in Figure 2F and G. These findings suggest that icariin plays a substantial role in the regulation of the MITF/Rab27A signaling axis in osteoclasts.

miRNA Characterization in ICA-OC-Exo and Verification of Significantly DEmiRNAs

The exosomes obtained from the cultural medium of osteoclasts in both the control group and icariin treatment groups were characterized (Figure 3A). In the control group, the exosome yield was 1.85 ± 0.09 μg per mL of culture medium of osteoclasts, whereas in the icariin treatment groups, it was 3.29 ± 0.12 μg. Morphological analysis using transmission electron microscopy revealed that the isolated exosomes exhibited a typical spherical and "saucer-like" structure. Nanoparticle tracking analysis of OC-Exo indicated a median particle size of 110–115 nm, falling within the expected range for exosomes (Figure 3B). These findings confirm the successful isolation of OC-Exo. CD9, CD63, and CD81 are key exosomal surface proteins. Western blot results showed these markers were highly expressed in both OC-Exo and ICA-OC-Exo. Calnexin, an endoplasmic reticulum marker and negative exosomes indicator, was absent in the extracted exosomes, indicating high purity (Figure 3C). In consideration of the contrasting exosomal secretion characteristics of OC-Exo and ICA-OC-Exo (Figure 3D),

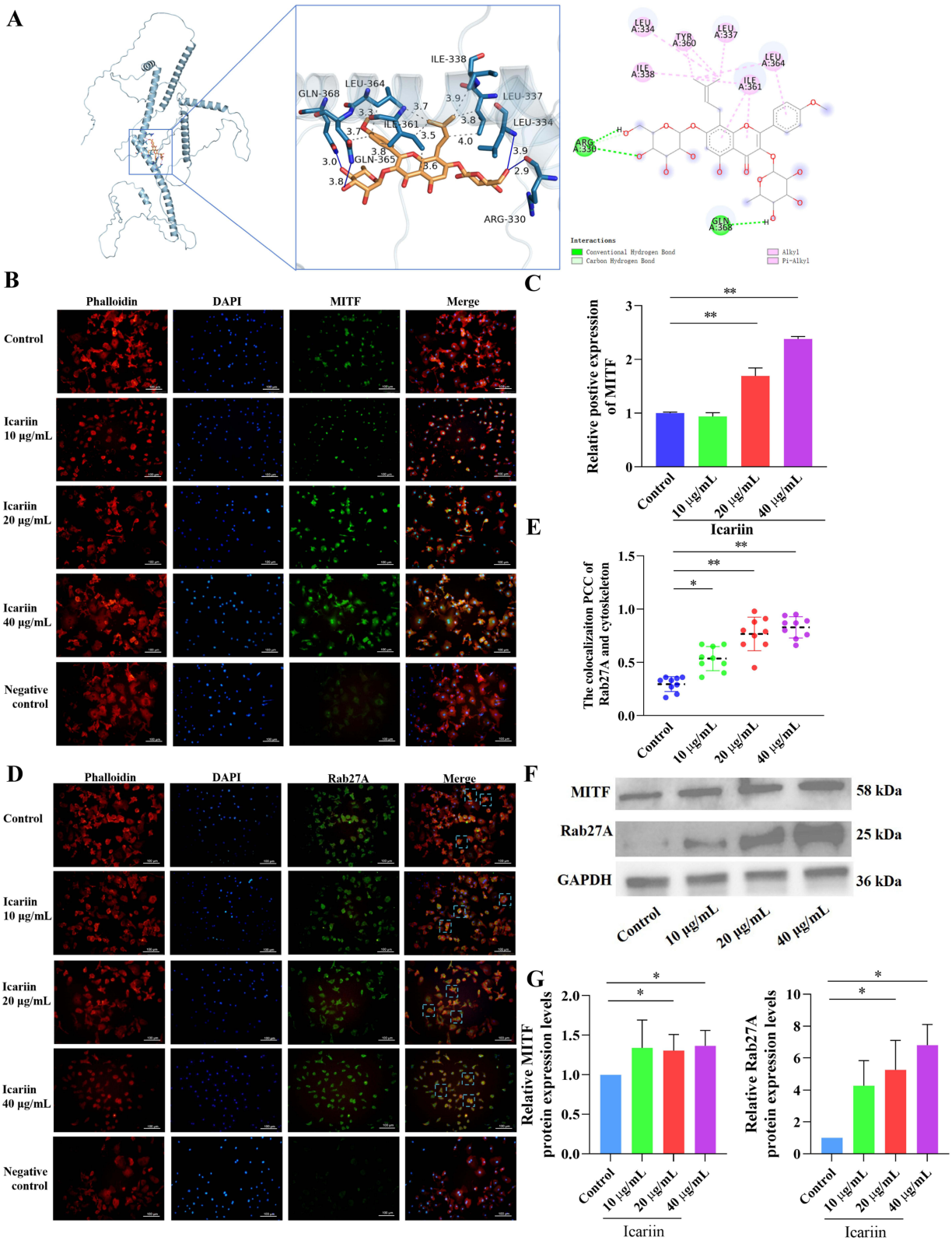

Figure 2 Icariin regulated MITF/Rab27A in osteoclasts. (**A**) Molecular docking between icariin and MITF. In the 3D plot, the blue solid line represents the hydrogen bond, the gray dotted line represents the hydrophobic force, in the 2D plot, the pink solid line represents the hydrophobic force, and the green and light green dotted lines both represent the hydrogen bond. (**B**) Representative images of immunofluorescence staining of MITF (green). The nucleus was stained with DAPI, and cytoskeleton were stained with phalloidin. (**C**) The histogram represents the relative positive expression of MITF in each group. $^{**}P < 0.01$ compared with the control groups. (**D**) Representative images of immunofluorescence staining of Rab27A (green). The nucleus was stained with DAPI, and cytoskeleton were stained with phalloidin. (**E**) The colocalization Pearson correlation coefficient (PCC) of Rab27A and cytoskeleton. Each dot represents the PCC per view under the microscope, and mean is indicated in black dotted lines. $^{*}P < 0.05$, $^{**}P < 0.01$ compared with the control groups. (**F** and **G**) Western Blot was used to test the protein expressions of MITF and Rab27A in osteoclasts treating with icariin, $^{*}P < 0.05$, compared with the control groups.

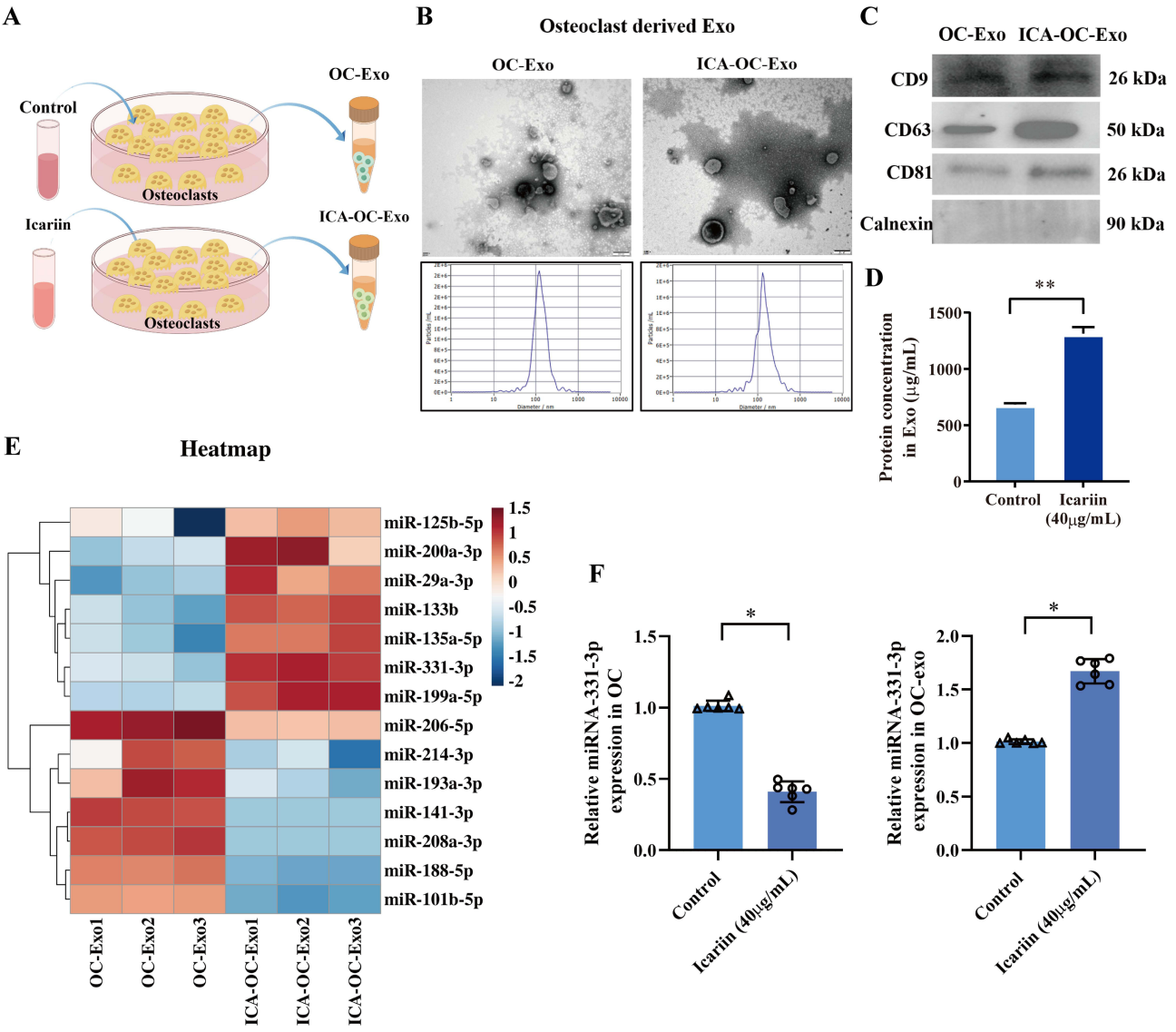

Figure 3 Characterization of OC-Exo and miRNAs in OC-Exo and comprehensive analysis. (**A**) The flow chart of extracting program OC-Exo and ICA-OC-Exo treating with control medium and icariin-containing medium. (**B**) Observation of exosomes derived from osteoclasts cultural medium by transmission electron microscopy, bar: 100 nm (upper). Size and concentration of exosomes by nanoparticle tracking analysis (lower). (**C**) The identification of postive and negative markers of exosomes through Western Blot analysis. (**D**) The total protein concentrations in OC-Exo and ICA-OC-Exo were measured following ultracentrifugation and resuspension in PBS, $^{**}P < 0.01$, compared with the control groups. (**E**) Clustering heat map of DEmiRNAs in OC-Exo and ICA-OC-Exo. (**F**) Relative miRNA-331-3p expressions in osteoclasts and OC-Exo treating with control cell culture medium and icariin-containing medium, $^{*}P < 0.05$, compared with the control groups.

we adhered to the standard protocols provided by Illumina for library preparation and sequencing analyses. Utilizing an Illumina HiSeq 2500 platform, we conducted miRNA expression profiling in OC-Exo and ICA-OC-Exo samples. The miRNA-seq data revealed the presence of 14 differentially expressed miRNAs (DEmiRNAs) ($P < 0.05$) between the OC-Exo and ICA-OC-Exo cohorts, as illustrated in Figure 3E. In order to assess the reproducibility of miRNA sequencing results, a quantitative real-time polymerase chain reaction (RT-qPCR) analysis was conducted on miRNAs exhibiting significant differences between OC-Exo and ICA-OC-Exo. The statistical findings were in concordance with the sequencing data, indicating a high level of agreement. Specifically, ICA-OC-Exo demonstrated an up-regulation in the expression of rno-miR-331-3p compared to the OC-Exo groups, as illustrated in Figure 3F.

Icariin Training OC-Exo Promoted the Proliferation of Osteoblasts

To investigate the impact of OC-Exo and ICA-OC-Exo on osteoblasts, a co-culture experiment was conducted by combining OC-Exo with osteoblasts (Figure 4A). Initially, exosomes derived from osteoclasts were labeled with PKH67, while osteoblasts were

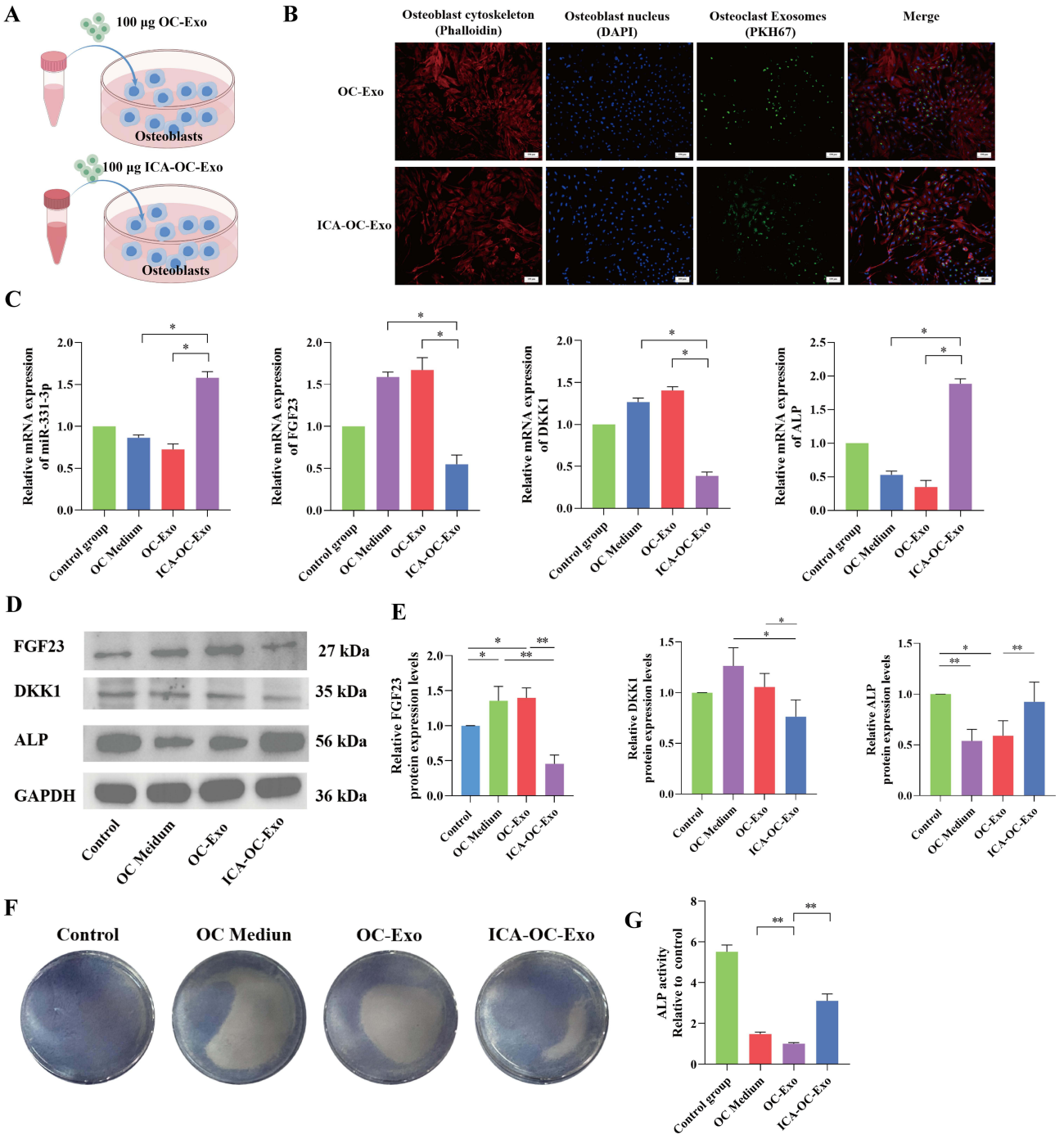

Figure 4 ICA-OC-Exo Promoted the Proliferation of Osteoblasts. (**A**) The diagrams of co-coculture OC-Exo or ICA-OC-Exo with osteoblasts. (**B**) Representative images of immunofluorescence staining of OC-Exo penetrating into osteoblasts. The OC-Exos were stained with PKH76 (green), the nucleuses of osteoblasts were stained with DAPI, and cytoskeleton were stained with phalloidin. (**C**) RT-qPCR was used to detect the gene expressions of miRNA-331-3p, FGF23, DKK1 and ALP in osteoblasts, $^{*}P < 0.05$. (**D** and **E**) Western Blot was used to test the protein expressions of FGF23, DKK1 and ALP in osteoblasts, $^{*}P < 0.05$, $^{**}P < 0.01$. (**F** and **G**) ALP staining and ALP activities were determined the effect of OC-Exo and ICA-OC-Exo on the proliferation of osteoblasts, $^{**}P< 0.01$.

stained with DAPI and phalloidin. The fluorescent images of OC-Exo and osteoblasts indicated the uptake of OC-Exo and ICA-OC-Exo by osteoblasts (Figure 4B). The RT-qPCR analysis revealed a significant increase in miRNA expression levels of miR-331-3p after 24 hours of treatment with ICA-OC-Exo (P <0.05), accompanied by a decrease in mRNA expression levels of FGF23 and DKK1. Furthermore, the study demonstrated a significant increase in alkaline phosphatase (ALP) levels following treatment with ICA-OC-Exo ($P < 0.05$) (Figure 4C). Western blot analysis revealed that ICA-OC-Exo led to higher protein

expression levels of osteogenic markers ALP compared to OC-Exo, while also reducing protein expression levels of FGF23 and DKK1 ($P < 0.05$) (Figure 4D and E). Subsequent ALP staining results after 24 hours of treatment with OC-Exo and ICA-OC-Exo on osteoclasts indicated a significant increase in osteoblast activity with ICA-OC-Exo treatment, with statistical significance ($P < 0.01$) (Figure 4F and G). These results showed that ICA-OC-Exo promoted osteoblast activity.

To investigate the modulation mechanism of miRNA-331-3p derived from OC-Exo and ICA-OC-Exo on osteoblast function, we employed a miRNA-331-3p inhibitor to knockdown miRNA-331-3p expression in osteoblasts, using a negative control (N.C.) for comparison (Figure 5A). RT-qPCR analysis demonstrated a significant reduction in miRNA-331-3p

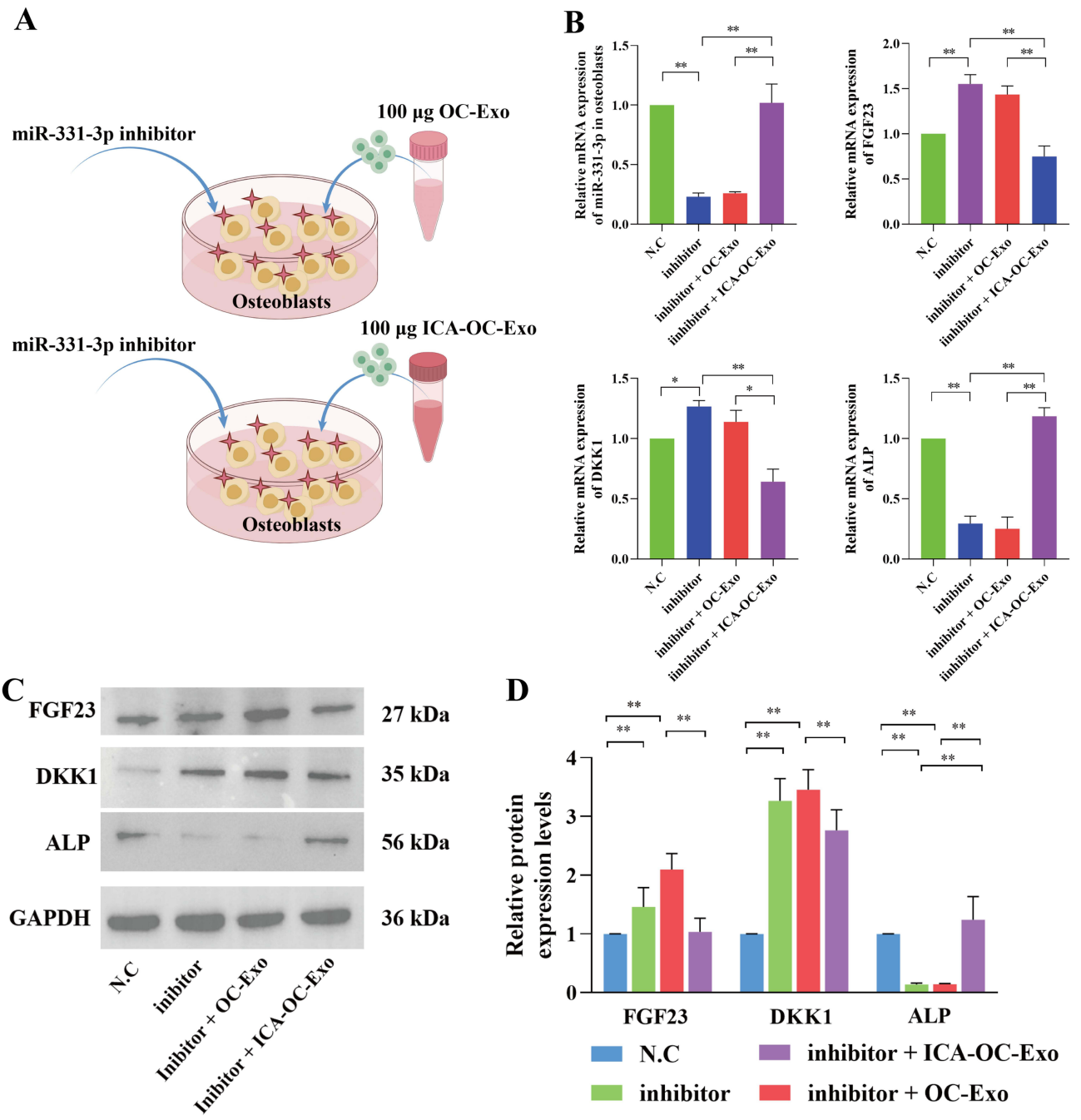

Figure 5 ICA-OC-Exo facilitated the proliferation of miRNA-331-3p inhibitor-induced osteoblasts. (**A**) The diagrams of co-coculture OC-Exo or ICA-OC-Exo with osteoblasts, which were transfected with miNRA-331-3p inhibitor. (**B**) RT-qPCR was used to detect the gene expressions of miRNA-331-3p, FGF23, DKK1 and ALP in osteoblasts, *$P < 0.05$, **$P < 0.01$. (**C** and **D**) Western Blot was used to test the protein expressions of FGF23, DKK1 and ALP in osteoblasts, *$P < 0.05$, **$P < 0.01$.

expression levels in the inhibitor group. Furthermore, after treatment with OC-Exo and ICA-OC-Exo, miR-331-3p levels were significantly higher in the inhibitor + ICA-OC-Exo group than those in the inhibitor + OC-Exo group ($P < 0.01$), which was accompanied by an increase in the mRNA expression levels of FGF23 and DKK1. Moreover, the study indicated a significant elevation in ALP levels following treatment with inhibitor + ICA-OC-Exo ($P < 0.05$, $P < 0.01$) as illustrated in Figure 5B. Western blot analysis demonstrated that the miRNA-331-3p inhibitor and OC-Exo treatment resulted in increased protein expression levels of the osteogenic markers FGF23 and DKK1 compared to the N.C. group, while concurrently decreasing the protein expression levels of ALP ($P < 0.01$). Additionally, the inhibitor + ICA-OC-Exo was associated with reduced expressions of FGF23 and DKK1, alongside an elevated expression of ALP, as depicted in Figure 5C and D. The results indicated that in osteoblasts where miRNA-331-3p was inhibited, ICA-OC-Exo facilitated enhanced osteoblast activity by delivering increased levels of miRNA-331-3p and suppressing FGF23.

ICA-OC-Exo Improved Bone Microarchitecture in Infected Bone Nonunion Rat Model

The efficacy of ICA-OC-Exo in promoting osteoblasts was demonstrated through its injection into bone defects in an infected bone nonunion rat model following the implantation of VSC beads (Figure 6A). Micro-CT analysis revealed that the bone microarchitecture of rats in the VCS+ICA-OC-Exo group exhibited significant improvement compared to the model group and VCS+OC-Exo group, at the 3-week and 6-week time points. At the 3-week mark, the BV/TV and BMD values of rats in the model and VCS groups were significantly lower than those in the control group, whereas the values in the VCS+ICA-OC-Exo group were notably higher than those in the VCS and VCS+OC-Exo groups. At the 6-week time point, the BV/TV and BMD values in the VCS+ICA-OC-Exo group remained significantly higher than those in the VCS and VCS+OC-Exo groups. Furthermore, the VCS+OC-Exo treatment significantly reduced the BV/TV and BMD values compared to the VCS treatment, indicating that OC-Exo inhibited bone repair, as shown in Figure 1D and depicted in Figure 6B and C. These results suggested that after anti-infection treatment of VSC in infected bone nonunion rat model, OC-Exo had negative effect on bone repair, and ICA-OC-Exo had the ability to attenuate bone repair at the local bone defect.

In order to elucidate the mechanism by which ICA-OC-Exo enhances bone formation, we conducted an investigation into the expression of OCN and FGF23 at the site of bone defect in a rat model of infected bone nonunion using immunofluorescence labeling, at the 3-week and 6-week time points. At the 3-week interval, a reduction in the number of OCN-positive cells was observed in the model group compared to the control group. Treatment with VSC, VSC+OC-Exo, and VSC+ICA-OC-Exo resulted in a significant increase in OCN expression. Furthermore, ICA-OC-Exo treatment led to a higher percentage of OCN-positive cells compared to the OC-Exo group. The proportion of FGF23-positive osteoblasts was assessed, indicating no significant differences among the VSC, VSC+OC-Exo, and VSC+ICA-OC-Exo treatment groups. At the 6-week mark, the ICA-OC-Exo treatment resulted in a significantly higher percentage of OCN-positive cells compared to the OC-Exo group. Furthermore, the VSC and VSC+OC-Exo treatments were associated with an increase in FGF23-positive osteoblasts. However, the VSC+ICA-OC-Exo treatment resulted in a lower number of FGF23-positive osteoblasts (Figure 7A and B). These findings suggest that ICA-OC-Exo treatment may decrease FGF23 expression in osteoblasts at the site of bone defect, ultimately promoting osteoblast mineralization.

Discussion

Bone infection presents a significant challenge in the field of orthopedic and traumatic surgery. Currently, the use of local implantation with an antibiotic release system has proven to be an efficacious approach for infection control. Nevertheless, the issue of delayed bone healing remains prevalent in clinical settings. Consequently, post-anti-infection treatment bone repair is imperative for the successful rehabilitation of patients suffering from bone infections. Previous studies showed that flavonoids are the active components in *Herba epimedii*. For instances, icariin and epimedins can suppress osteoclastogenesis in ovariectomized mice, promote osteoblast differentiation, and inhibit osteoclast differentiation.[32,33] Icariin can reduce bone loss in ovariectomized animal models and in hydrocortisone-induced rat models.[34] In our previous studies, we revealed that total flavonoids of *Herba epimedii* enhanced bone remolding in rabbit bone infected models and promoted activities of osteoblasts.[35] This study examined rat bone infected models and verified that icariin promoted bone repair after anti-infection

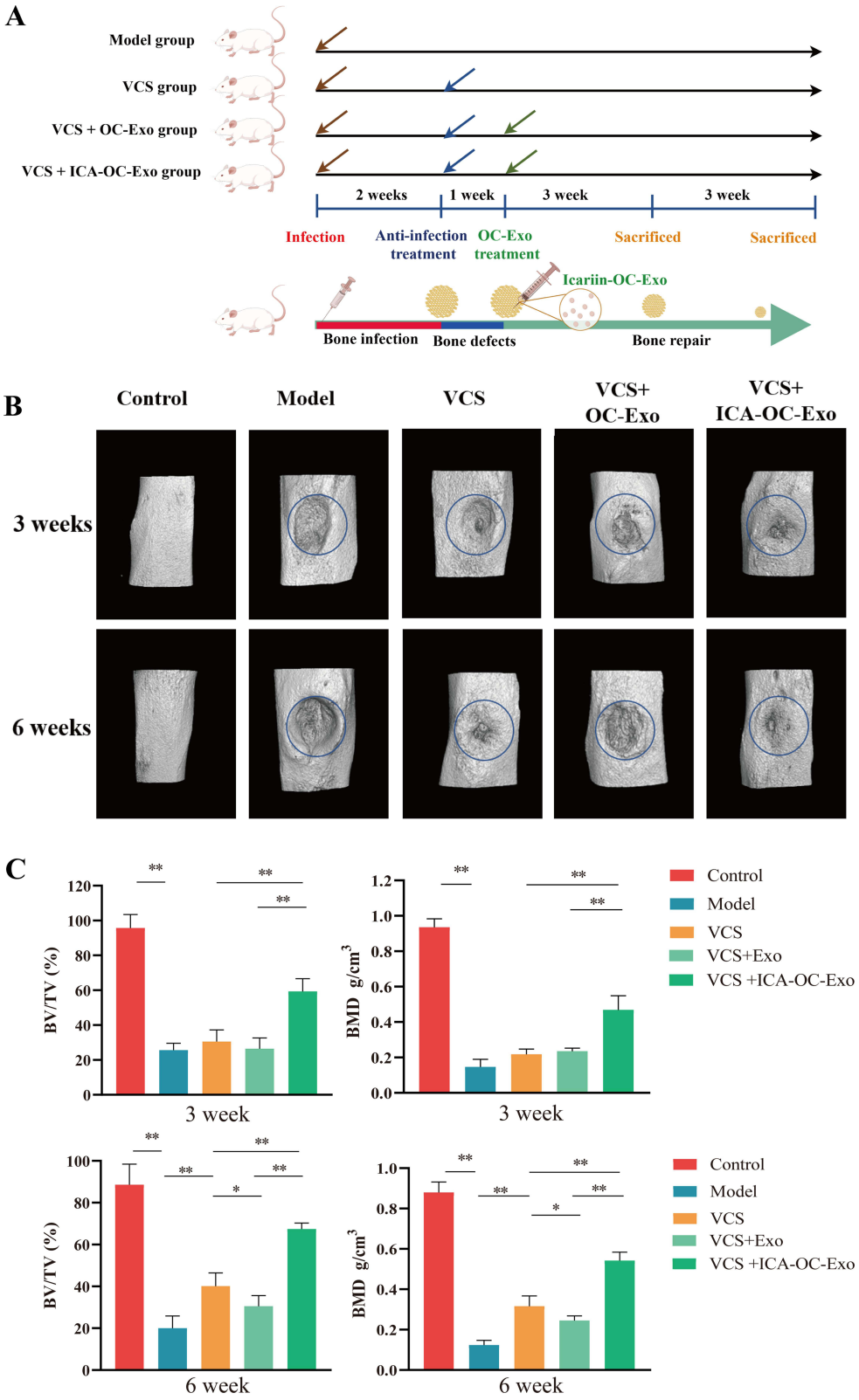

Figure 6 ICA-OC-Exo improved bone microarchitecture in infected bone nonunion rat model. (**A**) The diagrams of ICA-OC-Exo on infected bone nonunion rat model. (**B**) Appearance of bone defects on rats, and three-dimensional reconstruction of the tibia in each treatment group, at the 3-week and 6-week time points. The blue circles mean region of interest (ROI, 2mm diameters). (**C**) Histomorphometry parameters obtained by micro-CT included bone volume fraction (BV/TV), bone mineral density (BMD), at the 3-week and 6-week time points. Error bars indicate SD (n = 6), *$P < 0.05$, **$P < 0.01$.

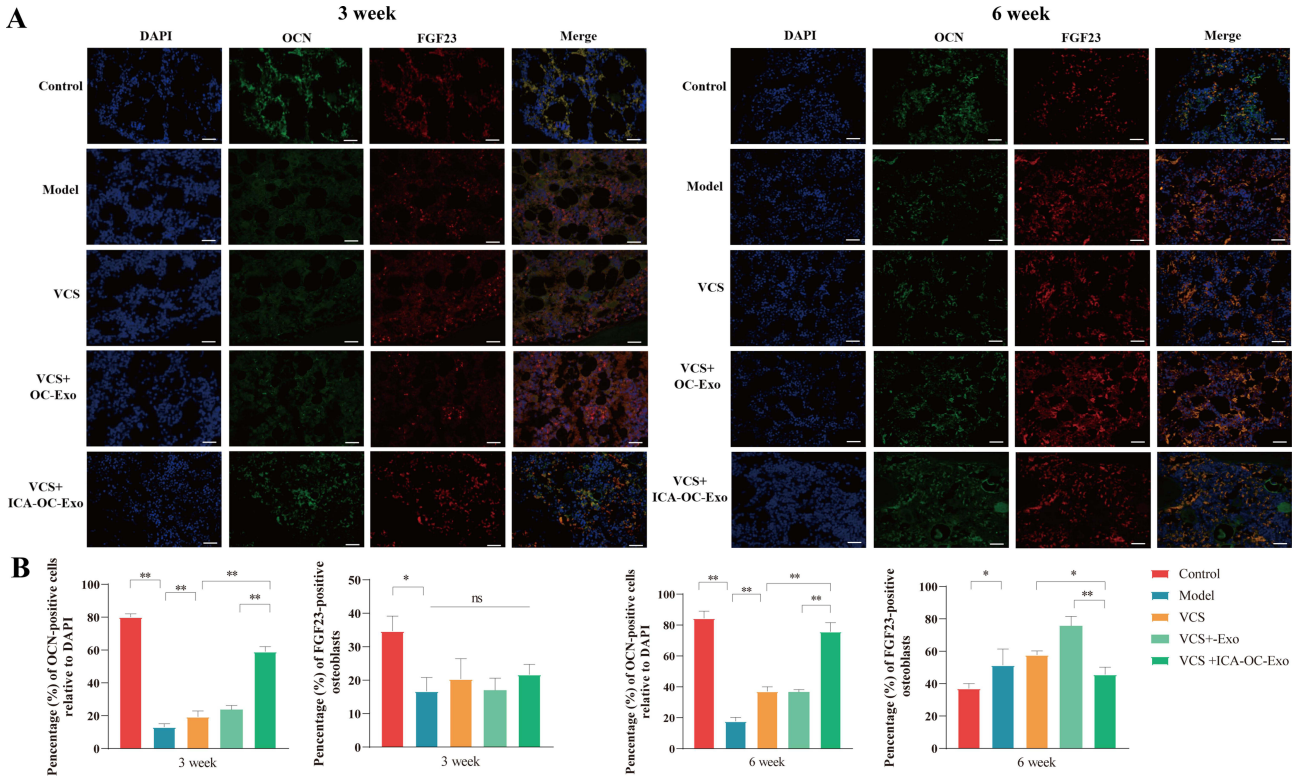

Figure 7 The effects of ICA-OC-Exo on OCN and FGF23 expression in a rat model of infected bone nonunion. (**A**) Immunofluorescence images depict bone tissue in each group, with antibodies targeting FGF23 (in red) and OCN (in green) in conjunction with DAPI-stained cell nuclei (in blue), at the 3-week and 6-week time points. (scale bars: 100 μm). (**B**) Quantitative analysis reveals a significant increase in OCN-positive cells and a decrease in FGF23-positive osteoblasts, at the 3-week and 6-week time points. Statistical significance is denoted as $^{*}P < 0.05$ and $^{**}P < 0.01$.

treatment. Icariin treatment increased BMD and bone volume at local bone defects. According to the histological results, icariin increased osteoblast numbers and decreased osteoclast numbers, and also inhibited CTSK expression, which indicated icariin suppressed bone repair osteoclast activity.

Prior research on the pathological mechanisms of bone infection has indicated that bone nonunion may be associated with an imbalance between bone formation and resorption, resulting from the upregulation of inflammatory factors that stimulate osteoblasts to secrete excessive RANKL. The interaction between RANKL and RANK promotes osteoclast differentiation.[12] Exosomes have been shown to play a role in mediating communication between osteoclasts and osteoblasts in the coupling mechanism of bone formation and resorption.[36] Osteoclasts can release exosomes loading various mRNA and non-coding RNA, and then the exosomes penetrated into osteoblasts and regulated biological function of osteoblasts.[37,38] Exosomes formation begins with early endosomes on the surface of cell membranes, which develop into late endosomes containing multiple ILVs that form MVB, the precursor of exosomes, by binding proteins, nucleic acids and other substances as the endogenous bud formation.[39] The secretory type of MVBs secretes exosomes to exocytosomes through fusion with the plasma membrane, and also ILVs are released as exosomes.[40] In this investigation, it was determined that icariin exhibited inhibitory effects on osteoclast activity, promoted an increase in the number of MVBs present in the cytoplasm, and facilitated the fusion of MVBs with plasma membranes. Nevertheless, icariin did not impact the quantification of ILVs within MVBs. As a result, it is postulated that icariin may modulate the secretion of osteoclast exosomes by regulating the process of exosome release.

The Rab family GTPase proteins control the transport process of intracellular MVBs, by collecting specific receptor proteins on the plasma membrane, which regulate exosomes secretion.[41] The Rab family GTPase proteins consist of Rab11, Rab35, Rab27A/B, etc. Studies have shown Rab27A and Rab27B are key proteins in the exosome's secretion process. Rab27A promotes the fusion of MVBs with the plasma membrane by binding to Slp4-a, the receptor of Rab27a on the plasma membrane. Rab27B regulates the movement of MVBs by binding to the receptor of Slac-2b.[42] Other

studies have shown that the expression of Rab27A is significantly increased, while the expression of Rab27B is significantly decreased during osteoclast differentiation. Also, Rab27A can regulate the multinucleation of osteoclasts by regulating cell membrane surface receptors.[43] On the other hand, MITF is verified to regulate the distribution of melanosomes in melanoma cells through transcriptional regulation of Rab27A and promote the extracellular secretion of melanosomes.[17] The findings of our research suggest that the stable binding of icariin to MITF is facilitated by molecular docking interactions. Furthermore, immunofluorescence staining results propose that MITF may regulate Rab27A and promote the extracellular secretion of MVBs. Additionally, Rab27A appears to localize away from the cytoskeleton after treatment with 20μg/mL and 40 μg/mL icariin. These results indicate that icariin plays a significant role in modulating the MITF/Rab27A signaling axis in osteoclasts. These findings suggest that icariin may have a potential impact on exosomes derived from osteoclasts, leading to an increase in the quantification of exosomes. These findings suggest that icariin may have a potential impact on exosomes derived from osteoclasts, leading to an increase in the quantification of exosomes.

MiRNAs present in exosomes play a crucial role in modulating the translation of target mRNA within receptor cells, thereby influencing the pathophysiological processes of said cells.[44] The miRNA-seq analysis revealed variations in miRNA expression levels between ICA-OC-Exo and OC-Exo samples, with miRNA-331-3p showing significantly elevated expression in ICA-OC-Exo. Additionally, it has been shown that miRNA-331-3p displays diminished expression levels throughout the process of osteoclast differentiation and proliferation. These findings align with existing literature, indicating substantial variations in the types of miRNAs present in exosomes following various drug interventions.[22] In our previous study, we investigated the miRNA biomarkers associated with bone infection and identified miRNA-331-3p as a regulator of osteoblast activity, contributing to bone nonunion. We observed an inverse correlation between miRNA-331-3p and fibroblast growth factor 23 (FGF23) in relation to osteoblast mineralization pathways and the pathology of infected bone nonunion. Specifically, miRNA-331-3p functions as a promoter of osteoblast mineralization by directly targeting FGF23. The downregulation of miRNA-331-3p was found to inhibit osteoblast mineralization through the regulation of DKK1/β-catenin-mediated signaling Therefore the miRNA-331-3p biomarker has been shown to regulate osteoblast mineralization through its targeting of FGF23. This novel mechanism presents potential as a diagnostic biomarker and therapeutic target for infected bone nonunion and other inflammatory bone disorders.[14] Subsequent co-culturing experiments involving ICA-OC-Exo or OC-Exo with osteoblasts demonstrated that ICA-OC-Exo significantly promotes osteoblast activity by downregulating FGF23 and DKK1, while upregulating ALP expressions. These findings suggest that icariin modulates cell communication between osteoclasts and osteoblasts by influencing the expression of miRNAs within exosomes released by osteoclasts.

Ultimately, ICA-OC-Exo was utilized to address bone defects in animals with infections, administered via local injection. Interestingly, OC-Exo was found to hinder bone formation and delay bone union, whereas ICA-OC-Exo demonstrated an increase in bone volume and bone mineral density (BMD). These findings suggest that ICA-OC-Exo has a significant impact on bone repair, particularly in cases where traditional methods have limited efficacy following anti-infection treatment. Additionally, in a separate study, icariin was incorporated into exosomes and utilized as a nanomedicine, showing promising results.[26,45] Furthermore, researchers have utilized icariin as a stimulus for exosomes in various cell types.[46] Our study also confirmed that icariin enhanced the quantification of exosomes derived from osteoclasts and altered the miRNAs within these exosomes. In vivo experimentation demonstrated that ICA-OC-Exo exhibited a significant impact on bone repair, suggesting a promising treatment approach for bone defects.

Our findings offer a novel concept and foundation for developing an icariin-induced osteoclast exosome for addressing bone defects, as well as potentially informing research on flavonoid-induced osteoclast exosomes. Nevertheless, our investigation did not validate the role of FGF23 in eliminating osteoblast-derived exosomes both in vitro and in vivo. Furthermore, the in vivo distribution and metabolism of ICA-OC-Exo remain ambiguous, necessitating additional research. Although our study found no side effects in rats treated with ICA-OC-Exo over a 6-week period, further research is necessary to conduct long-term safety assessments. Exosomes serve as effective carriers of RNA, facilitating the efficient delivery of RNA to target cells and thereby enhancing the efficacy of RNA-based therapeutics.[47] However, the limited quantification of exosomes derived from donor cells poses a significant challenge to their clinical application. Previous studies have demonstrated that factors such as hypoxia, inflammation, and the administration of small molecules or traditional Chinese medicine extracts can augment the quantification of exosomes and alter their

miRNA composition.[48] Our findings demonstrated that icariin can alter the quantification and miRNA profile of OC-Exo, providing valuable insights into the production of abundant and function-specific exosomes. These insights could significantly contribute to the development of function-specific exosomes for clinical trials. Moreover, we propose that ICA-OC-Exo holds potential applicability in the treatment of various bone disorders, including osteoporosis. Osteoporosis is typified by heightened osteoclast activity and diminished osteoblast function.[49] The localized administration of ICA-OC-Exo could potentially modulate the progression of osteoporosis. Therefore, it is crucial to conduct further research to explore the therapeutic efficacy of ICA-OC-Exo in managing disorders of the skeletal system.

Conclusions

The current study revealed that icariin promotes the secretion of osteoclast exosomes via a MITF/RAB27A-dependent pathway and upregulates miRNA-331-3p within the icariin-induced OC-Exo. The ICA-OC-Exo subsequently influences the activity of osteoblasts. These results propose a potential mechanism through which icariin aids in bone regeneration post anti-infection treatment for bone infections, suggesting the potential utility of ICA-OC-Exo as an innovative therapeutic strategy for addressing bone deficiencies. Furthermore, comprehensive in vivo investigations into the metabolism and distribution of ICA-OC-Exo, along with assessments of the long-term effects associated with its use, are planned for future implementation.

Ethics Statement

The animal study was reviewed and approved by Animal Ethics Committee of Zhejiang Academy of Traditional Chinese Medicine, and conformed to the ARRIVE guidelines (Approval No. [2022]005)

Author Contributions

All authors made a significant contribution to the work reported, whether that is in the conception, study design, execution, acquisition of data, analysis and interpretation, or in all these areas; took part in drafting, revising or critically reviewing the article; gave final approval of the version to be published; have agreed on the journal to which the article has been submitted; and agree to be accountable for all aspects of the work.

Funding

This study was supported by the Nature Science Foundation of Zhejiang Province (grant no. LD22C060002), National Science Foundation of China (grant no. 82474240, 82274547), Zhejiang Provincial Medical and Health Science and Technology Fund (grant no. 2024KY1223), Research Project of Zhejiang Chinese Medical University (grant no. 2023JKZKTS34), Project of Chunyan Special Fund for Chinese Medicine Development of Zhejiang Chinese Medical University (grant no. CY202305).

Disclosure

The authors declare that the research was conducted in the absence of any commercial or financial relationships that could be construed as a potential conflict of interest.

References

1. Masters EA, Ricciardi BF, Bentley KL, et al. Skeletal infections: microbial pathogenesis, immunity and clinical management. *Nat Rev Microbiol*. 2022;20(7):385–400. doi:10.1038/s41579-022-00686-0
2. Lu H, Liu Y, Guo J, Wu H, Wang J, Wu G. Biomaterials with antibacterial and osteoinductive properties to repair infected bone defects. *Int J Mol Sci*. 2016;17(3):334. doi:10.3390/ijms17030334
3. Ren Y, Liu L, Sun D, et al. Epidemiological updates of post-traumatic related limb osteomyelitis in China: a 10 years multicentre cohort study. *Int J Surg*. 2023;109(9):2721–2731. doi:10.1097/JS9.0000000000000502
4. Hu X, Chen J, Yang S, et al. 3D printed multifunctional biomimetic bone scaffold combined with TP-Mg nanoparticles for the infectious bone defects repair. *Small*. 2024;20(40):e2403681. doi:10.1002/smll.202403681
5. Cao Z, Qin Z, Duns GJ, et al. Repair of infected bone defects with hydrogel materials. *Polymers*. 2024;16(2):281. doi:10.3390/polym16020281
6. Gimza BD, Cassat JE. Mechanisms of antibiotic failure during Staphylococcus aureus osteomyelitis. *Front Immunol*. 2021;12:638085. doi:10.3389/fimmu.2021.638085
7. Krishnan AG, Biswas R, Menon D, et al. Biodegradable nanocomposite fibrous scaffold mediated local delivery of vancomycin for the treatment of MRSA infected experimental osteomyelitis. *Biomater Sci*. 2020;8(9):2653–2665. doi:10.1039/d0bm00140f

8. Kavanagh N, Ryan EJ, Widaa A, et al. Staphylococcal osteomyelitis: disease progression, treatment challenges, and future directions. *Clin Microbiol Rev*. 2018;31(2):e00084–17. doi:10.1128/CMR.00084-17
9. Perisano C, Cianni L, Polichetti C, et al. Plate augmentation in aseptic femoral shaft nonunion after intramedullary nailing: a literature review. *Bioeng*. 2022;9(10):560. doi:10.3390/bioengineering9100560
10. Pearson JJ, Gerken N, Bae C, et al. In vivo hydroxyapatite scaffold performance in infected bone defects. *J Biomed Mater Res B Appl Biomater*. 2020;108(3):1157–1166. doi:10.1002/jbm.b.34466
11. Qian H, Yao Q, Pi L, et al. Current advances and applications of tantalum element in infected bone defects. *ACS Biomater Sci Eng*. 2023;9(1):1–19. doi:10.1021/acsbiomaterials.2c00884
12. Kim JM, Lin CJ, Stavre ZN, Greenblatt MB, Shim JH. Osteoblast-osteoclast communication and bone homeostasis. *Cells*. 2020;9(9):2073. doi:10.3390/cells9092073
13. Zhang Y, Shen L, Wang P, et al. Treatment with vancomycin loaded calcium sulphate and autogenous bone in an improved rabbit model of bone infection. *J Vis Exp*. 2019;14(145):e57294. doi:10.3791/57294
14. Zhang Y, Wang X, Huang X, et al. Transcriptome sequencing profiling identifies miRNA-331-3p as an osteoblast-specific miRNA in infected bone nonunion. *Bone*. 2021;143:115619. doi:10.1016/j.bone.2020.115619
15. Garcia-Martin R, Wang G, Brandão BB, et al. MicroRNA sequence codes for small extracellular vesicle release and cellular retention. *Nature*. 2022;601(7893):446–451. doi:10.1038/s41586-021-04234-3
16. Alexander M, Ramstead AG, Bauer KM, et al. Rab27-dependent exosome production inhibits chronic inflammation and enables acute responses to inflammatory stimuli. *J Immunol*. 2017;199(10):3559–3570. doi:10.4049/jimmunol.1700904
17. George A, Zand DJ, Hufnagel RB, et al. Biallelic mutations in MITF cause coloboma, osteopetrosis, microphthalmia, macrocephaly, albinism, and deafness. *Am J Hum Genet*. 2016;99(6):1388–1394. doi:10.1016/j.ajhg.2016.11.004
18. Sims NA, Martin TJ. Osteoclasts provide coupling signals to osteoblast lineage cells through multiple mechanisms. *Annu Rev Physiol*. 2020;82(1):507–529. doi:10.1146/annurev-physiol-021119-034425
19. Fang F, Yang J, Wang J, et al. The role and applications of extracellular vesicles in osteoporosis. *Bone Res*. 2024;12(1):4. doi:10.1038/s41413-023-00313-5
20. Jeppesen DK, Zhang Q, Franklin JL, Coffey RJ. Extracellular vesicles and nanoparticles: emerging complexities. *Trends Cell Biol*. 2023;33(8):667–681. doi:10.1038/s41413-023-00313-5
21. Dixson AC, Dawson TR, Di Vizio D, et al. Context-specific regulation of extracellular vesicle biogenesis and cargo selection. *Nat Rev Mol Cell Biol*. 2023;24(7):454–476. doi:10.1038/s41580-023-00576-0
22. Cha KY, Cho W, Park S, et al. Generation of bioactive MSC-EVs for bone tissue regeneration by tauroursodeoxycholic acid treatment. *J Control Release*. 2023;354:45–56. doi:10.1016/j.jconrel.2022.12.053
23. Bai L, Liu Y, Zhang X, et al. Osteoporosis remission via an anti-inflammaging effect by icariin activated autophagy. *Biomaterials*. 2023;297:122125. doi:10.1016/j.biomaterials.2023.122125
24. Si Y, Li Y, Gu K, Yin H, Ma Y. Icariin ameliorates osteoporosis in ovariectomized rats by targeting Cullin 3/Nrf2/OH pathway for osteoclast inhibition. *Biomed Pharmacother*. 2024;173:116422. doi:10.1016/j.biopha.2024.116422
25. Yong EL, Cheong WF, Huang Z, et al. Randomized, double-blind, placebo-controlled trial to examine the safety, pharmacokinetics and effects of Epimedium prenylflavonoids, on bone specific alkaline phosphatase and the osteoclast adaptor protein TRAF6 in post-menopausal women. *Phytomedicine*. 2021;91:153680. doi:10.1016/j.phymed.2021.153680
26. Dong M, Wu S, Xu H, et al. FBS-derived exosomes as a natural nano-scale carrier for icariin promote osteoblast proliferation. *Front Bioeng Biotechnol*. 2021;9:615920. doi:10.3389/fbioe.2021.615920
27. Zeng J, Sun P, Zhao Y, et al. Bone mesenchymal stem cell-derived exosomes involved co-delivery and synergism effect with icariin via mussel-inspired multifunctional hydrogel for cartilage protection. *Asian J Pharm Sci*. 2023;18(3):100799. doi:10.1016/j.ajps.2023.100799
28. Laha D, Deb M, Das H. KLF2 (kruppel-like factor 2 [lung]) regulates osteoclastogenesis by modulating autophagy. *Autophagy*. 2019;15(12):2063–2075. doi:10.1080/15548627.2019.1596491
29. Liao X, Shen M, Li T, et al. Combined molybdenum gelatine methacrylate injectable nano-hydrogel effective against diabetic bone regeneration. *Int J Nanomed*. 2023;18:5925–5942. doi:10.2147/IJN.S428429
30. Lei SS, Huang XW, Li LZ, et al. Exploring the mechanism of epimedii folium-rhizoma drynariae herbal pair promoted bone defects healing through network pharmacology and experimental studies. *J Ethnopharmacol*. 2024;319(Pt 3):117329. doi:10.1016/j.jep.2023.117329
31. Bouxsein ML, Boyd SK, Christiansen BA, et al. Guidelines for assessment of bone microstructure in rodents using micro-computed tomography. *J Bone Miner Res*. 2010;25(7):1468–1486. doi:10.1002/jbmr.141
32. Li Z, Li D, Chen R, et al. Cell death regulation: a new way for natural products to treat osteoporosis. *Pharmacol Res*. 2023;187:106635. doi:10.1016/j.phrs.2022.106635
33. Ramesh P, Jagadeesan R, Sekaran S, et al. Flavonoids: classification, function, and molecular mechanisms involved in bone remodelling. *Front Endocrinol*. 2021;12:779638. doi:10.3389/fendo.2021.779638
34. Zhou L, Poon CCW, Wong KY, et al. Icariin ameliorates estrogen-deficiency induced bone loss by enhancing IGF-I signaling via its crosstalk with non-genomic ERα signaling. *Phytomedicine*. 2021;82:153413. doi:10.1016/j.phymed.2020.153413
35. Shou D, Zhang Y, Shen L, et al. Flavonoids of herba epimedii enhances bone repair in a rabbit model of chronic osteomyelitis during post-infection treatment and stimulates osteoblast proliferation in vitro. *Phytother Res*. 2017;31(2):330–339. doi:10.1002/ptr.5755
36. Zhang C, Pan L, Zhang H, et al. Osteoblasts-derived exosomal lncRNA-MALAT1 promotes osteoclastogenesis by targeting the miR-124/NFATc1 signaling axis in bone marrow-derived macrophages. *Int J Nanomed*. 2023;18:781–795. doi:10.2147/IJN.S395607
37. Pan L, Zhang C, Zhang H, et al. Osteoclast-derived exosomal miR-5134-5p interferes with alveolar bone homeostasis by targeting the JAK2/STAT3 Axis. *Int J Nanomed*. 2023;18:3727–3744. doi:10.2147/IJN.S413692
38. Mi B, Chen L, Xiong Y, et al. Osteoblast/osteoclast and immune cocktail therapy of an exosome/drug delivery multifunctional hydrogel accelerates fracture repair. *ACS Nano*. 2022;16(1):771–782. doi:10.1021/acsnano.1c08284
39. Hyenne V, Labouesse M, Goetz JG. The small GTPase Ral orchestrates MVB biogenesis and exosome secretion. *Small GTPases*. 2018;9(6):445–451. doi:10.1080/21541248.2016.1251378

40. Perrin P, Janssen L, Janssen H, et al. Retrofusion of intralumenal MVB membranes parallels viral infection and coexists with exosome release. *Curr Biol*. 2021;31(17):3884–3893.e4. doi:10.1016/j.cub.2021.06.022
41. Wilmes S, Kümmel D. Insights into the role of the membranes in Rab GTPase regulation. *Curr Opin Cell Biol*. 2023;83:102177. doi:10.1016/j.ceb.2023.102177
42. Song L, Tang S, Han X, et al. KIBRA controls exosome secretion via inhibiting the proteasomal degradation of Rab27a. *Nat Commun*. 2019;10(1):1639. doi:10.1038/s41467-019-09720-x
43. Tang L, Yuan L, Yan J, et al. circ_0029463 promotes osteoclast differentiation by mediating miR-134-5p/Rab27a axis. *J Orthop Surg Res*. 2024;19(1):128. doi:10.1186/s13018-024-04610-5
44. Krylova SV, Feng D. The machinery of exosomes: biogenesis, release, and uptake. *Int J Mol Sci*. 2023;24(2):1337. doi:10.3390/ijms24021337
45. Yan Q, Song C, Liu H, et al. Adipose-derived stem cell exosomes loaded with icariin attenuated M1 polarization of macrophages via inhibiting the TLR4/Myd88/NF-κB signaling pathway. *Int Immunopharmacol*. 2024;137:112448. doi:10.1016/j.intimp.2024.112448
46. Zhang S, Li Y, Wang Q. Icariin attenuates human renal tubular epithelial cell senescence by targeting PAK2 via miR-23b-3p. *Curr Pharm Biotechnol*. 2024;25(17):2278–2289. doi:10.2174/0113892010276372231129105022
47. Berger S, Lächelt U, Wagner E. Dynamic carriers for therapeutic RNA delivery. *Proc Natl Acad Sci U S A*. 2024;121(11):e2307799120. doi:10.1073/pnas.2307799120
48. Jeppesen DK, Fenix AM, Franklin JL, et al. Reassessment of exosome composition. *Cell*. 2019;177(2):428–445.e18. doi:10.1016/j.cell.2019.02.029
49. Hansen MS, Madsen K, Price M, et al. Transcriptional reprogramming during human osteoclast differentiation identifies regulators of osteoclast activity. *Bone Res*. 2024;12(1):5. doi:10.1038/s41413-023-00312-6

International Journal of Nanomedicine Dovepress

Publish your work in this journal

The International Journal of Nanomedicine is an international, peer-reviewed journal focusing on the application of nanotechnology in diagnostics, therapeutics, and drug delivery systems throughout the biomedical field. This journal is indexed on PubMed Central, MedLine, CAS, SciSearch®, Current Contents®/Clinical Medicine, Journal Citation Reports/Science Edition, EMBase, Scopus and the Elsevier Bibliographic databases. The manuscript management system is completely online and includes a very quick and fair peer-review system, which is all easy to use. Visit http://www.dovepress.com/testimonials.php to read real quotes from published authors.

Submit your manuscript here: https://www.dovepress.com/international-journal-of-nanomedicine-journal